RSC Advances

ROYAL SOCIETY OF CHEMISTRY

www.rsc.org/advances

Graph abstract

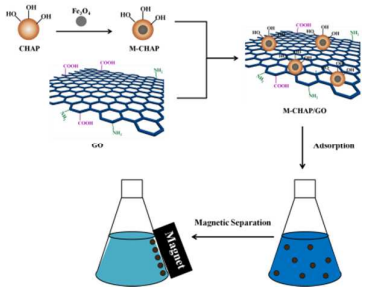

Magnetic carbonate hydroxyapatite was loaded onto GO sheets to get a novel adsorbent for removal of heavy metals and dye.

Mechanism of Pb(II) and methylene blue adsorption onto magnetic carbonate hydroxyapatite/graphene oxide

Limei Cui[a], Yaoguang Wang[b], Lihua Hu[b], Liang Gao[b], Bin Du[a*], Qin Wei[b]

[a] School of Resources and Environment, University of Jinan, Jinan 250022, China

[b] Key Laboratory of Chemical Sensing & Analysis in Universities of Shandong, School of Chemistry and Chemical Engineering, University of Jinan, Jinan 250022, China

* To whom all correspondence should be addressed

Tel: + 86-531-82767872

Fax: + 86-531-82767370

E-mail: dubin61@gmail.com (B. Du)

Mechanism of Pb(II) and methylene blue adsorption onto magnetic carbonate hydroxyapatite/graphene oxide

Abstract:

Magnetic carbonate hydroxyapatite/graphene oxide (M-CHAP/GO) was successfully prepared by loading magnetic carbonate hydroxyapatite (M-CHAP) onto graphene oxide sheet and found to be an ideal adsorbent for heavy metal (Pb(II)) and dye (methylene blue). The obtained adsorbent was characterized by SEM, FTIR, XRD, BET, TGA, XPS and Zeta potential, respectively. M-CHAP/GO nano-particles possessed a favorable and stable morphology. Moreover, the good magnetic properties of M-CHAP/GO made it simply recover from water with magnetic separation. The equilibrium adsorption capacity was 277.7 mg g^{-1} for Pb(II) and 546.4 mg g^{-1} for methylene blue under the optimal conditions, respectively. The pseudo-second-order equation and the Langmuir model showed good correlation with the experimental data and well explained the mechanism of adsorption. It was found that the adsorption process accomplished mainly via chelation and ion exchange. Thermodynamic studies ($\Delta G<0$, $\Delta H>0$, $\Delta S>0$) implied that the adsorption process was endothermic and spontaneous in nature. The other adsorption mechanisms were further researched in the article. All the experimental results show that M-CHAP/GO nano-particles have a potential application in the future environmental management.

Keywords: Magnetic CHAP/GO; Pb(II); Methylene blue; Isotherm; Kinetics

1. Introduction

Wastewater discharged from various human activities has causing serious threats to environment and drinking water. Heavy metals ions and dyes are two of the most basic environmental pollutants due to the indiscriminate disposal of wastewater[1]. Wastewaters from many industries, such as mining, metallurgical, chemical industry and battery manufacturing, contain plentiful kinds of toxic heavy metal ions[2]. They are non-biodegradable and accumulated in living organisms, causing various diseases and disorders[3]. Lead ions, for example, accumulate mainly in bones, brain, kidney and muscles and may cause some serious disorders like kidney disease, nervous disorders, anaemia and sickness even death[4]. The discharge of dyes into the environment is also worthy of concern for both toxicological and esthetical reasons. Textile, paper, leather and plastics industries are some of the sources for dye effluents[5]. Methylene blue (MB) is the most commonly used substance for dying cotton, wood or silk. Long-term surface contact with MB can give rise to permanent injury on the eyes. Moreover, long-term MB inhalation may cause nausea, vomiting and mental disorders, etc.[6]. The enormous harmfulness of heavy metals pollution and dye wastewater makes it particularly important to remove them from aqueous solution. Among several chemical or physical methods, adsorption has been found to be superior compared with other techniques (chemical precipitation, conventional coagulation, ion-exchange, line softening, reverse osmosis and so on) for wastewater treatment in terms of its simplicity of design, low cost and capability for efficiently adsorbing a broad range of pollutants[7-9]. In recent years, designing a suitable adsorbent for Pb(II) or MB removal

has attracted wide attention. What's more, some careless disposal behaviors probably bring about a mixture of the two kinds of pollutants, which surely increases the difficulty in the industrial wastewater treatment. So, it is significant to investigate an effective adsorbent to remove both lead and MB.

Hydroxyapatite (HAP) is a stable and inexpensive salt produced through precipitation from calcium phosphate solutions[10]. The structure of hydroxyapatite is hexagonal, with space group $P6_3/m$: essentially a 6-fold *c*-axis perpendicular to three equivalent *a*-axes at angles of 120° to each other. HAP is a principal component of animal hard tissues and shows excellent potential in water treatment because of its environment friendly nature, low cost, high stability and adsorption capacity for heavy metals[11, 12]. It has been reported in removal of a wide variety of metals (e.g., Cu, Cr, Co, Cd, Zn, Ni, Pb, As, Sb and Sr) by many investigators[9, 11, 13-18]. The adsorption takes place through ionic exchange reaction, surface complexation with phosphate, calcium and hydroxyl groups and/or co-precipitation. More recently, the synthetic carbonate hydroxyapatite (CHAP) had higher efficiency in the removal of heavy metals (Pb(II), Cd(II), Cu(II), Hg(II)) than HAP, but its dissolution, crystallizability, surface activity and thermal stability don't change much[19, 20].

However, there are still some shortcomings for CHAP in the application of adsorption. On the one hand, the tiny size of pure CHAP nano-particles may increase the burden of solid-liquid separation. Much effort has been made to modify CHAP nano-particles[21]. Magnetic nano-materials, like Fe_3O_4 nano-particles have drawn considerable attention because of their great potential applications in magnetic felids[22].

The use of a magnet can provide a very simple and effective method to separate the particles along with target pollutants from the aqueous phase. In principle, adsorption can remove heavy metals and then recover and recycle them back to industrial processes[23, 24]. With the help of magnetic materials, it will be easy to realize. Meanwhile, the excellent magnetic recycle performance of nano-materials can effectively avoid the release of nano-scale adsorbent into environment which may result in unknown damage [25]. If Fe_3O_4 can be introduced into CHAP, they will significantly improve the adsorption process. On the other hand, CHAP nano-particles are very limited in dye adsorption. Dye adsorption is mainly depended on the action of groups between dye and adsorbent or conjugation effect[26, 27]. The single hydroxyl groups on the surface of CHAP are not beneficial to react with most dyes. Compared with inorganic compounds, organic materials generally have a better affinity with dyes. Graphene oxides, which are considered as the oxidized graphene, contain oxygen-containing functional groups (-COOH, -OH, C=O) on the surfaces, these functional groups can widely react with MB as well as Pb(II)[28-30]. Considering the high surface area (theoretical value of 2620 m^2 g^{-1}) has attracted considerable attention as a two dimensional carbon-based material of atomic thickness[2], the graphene oxide nano-sheets should have high adsorption capacity in removal of dyes and heavy metals from large volumes of aqueous solutions.

From the above, developing adsorbents which combine the advantages of GO, Fe_3O_4 and CHAP will be an excellent method to clean up the heavy metals pollution and dye wastewater. The primary objective of this work is to develop magnetic

carbonate hydroxyapatite/graphene oxide (M-CHAP/GO) for heavy metals (Pb(II)) and dye (MB) adsorption, which can take full advantage of abundant oxygen-containing functional groups and large specific surface area of GO, strong ion exchange properties of CHAP and the magnetic separation performance of Fe_3O_4. In particular, the magnetic CHAP in such composite could also serve as a stabilizer against the aggregation of individual GO sheets due to a strong van der Waals interaction between the GO layers[31]. Therefore, M-CHAP/GO is potential to be a cost-effective adsorbent for removal of Pb(Ⅱ) and MB from wastewater. The present work investigated the influence of various parameters on the adsorption process and determined the optimum conditions. In addition, both adsorption behavior and mechanism were explored at the microcosmic level.

2. **Materials and methods**

2.1 Reagents and solutions

All chemicals in this experiment were from Sinopharm Chemical Reagent Beijing Co., Ltd, China, which are analytical reagent grade or better quality. The solutions were prepared with ultrapure water (EASY-pure LF, Barnstead International, Dubuque, Iowa USA).

2.2 Synthesis of M-CHAP/GO

Graphene oxide (GO) were prepared from purified natural graphite by the modified Hummers method[32]. Fe_3O_4 nano-particles were prepared by hydrothermal method[33]. M-CHAP/GO was prepared according to the following steps: Firstly, 300 mL of calcium nitrate (0.025 mol L^{-1}) was added into a three-necked round-bottomed

flask provided with a mechanical stirrer and heated to 45 °C. 38.42 mL of ammonium bicarbonate (0.3 mol L^{-1}) mixed with 174.65 mL of diammonium phosphate (0.3 mol L^{-1}). 0.1 g Fe_3O_4 nano-particles were dispersed in the above mixture by ultrasonic dispersion for 8 min. Then, the dispersion was slowly added into calcium nitrate solution dropwise. In this process, the pH of the mixed system was kept at 10 by using ammonia. The reaction was kept for 40 min at 45 °C under severe mechanical agitation. The last compounding step: 0.1 g GO was dispersed in 20 mL of ultrapure water by ultrasonic dispersion for 20 min and then added to the above reaction system, and then kept reacting at 45 °C for 5 h. After that, the obtained precipitate was aged for 24 h. The final product, named M-CHAP/GO, was collected by the aid of an adscititious magnet and dried in a vacuum oven at 50 °C for 24 h.

2.3 Characterization methods and instruments

The morphology of M-CHAP/GO was investigated by SEM images obtained from a field emission SEM (ZEISS, Germany). FTIR spectra were recorded in the spectral range of 4000-400 cm^{-1} on a Perkin-Elmer Spectrum One FTIR spectrometer (Perkin–Elmer, United States). XRD patterns were acquired with a Rigaku D/MAX 2200 X-ray diffractometer (Tokyo, Japan). BET analysis was performed on Micromeritics ASAP 2020 surface area and porosity analyzer (Quantachrome, United States). XPS analysis was performed on ESCALAB 250 (Thermo Fisher Scientific, USA). Pore distributions and pore volume were calculated using the adsorption branch of the N_2 isotherms based on the BJH model. The zeta potential was measured at various pH with a JS94H (Shanghai, China).

2.4 Batch adsorption experiments

All of pollutant solutions in the experiment were prepared by dissolving $Pb(NO_3)_2$ and MB into ultrapure water. Fresh dilutions were used in each experiment.

In order to determine the optimum adsorption conditions and study the adsorption mechanism of Pb(II) and MB adsorption, batch adsorption experiments were performed in 100 mL stopper conical flask and shaken on a temperature controlled shaker. The effect of dosage was tested in the range of 3-20 mg (natural pH, contact time for 3 h, temperature at 298 K). The effect of contact time was studied in the time range of 3-180 min (dosage of 10 mg for Pb(II) and 12 mg for MB, natural pH, temperature at 298 K). The effect of pH was investigated in the range of 3-8 for Pb(II) and 2-12 for MB. Adsorption equilibrium isotherms were carried out with the initial concentrations rang of 40-200 mg L^{-1} for Pb(II) and 30-300 mg L^{-1} for MB. Adsorption thermodynamics were conducted at temperatures ranging from 298 K to 318 K with varying initial concentration.

At the end of adsorption, M-CHAP/GO was separated from the solution by magnetic separation. Pollutant was determined by a UV-Vis spectrophotometer (TU-1901, Beijing Purkinje General Instrument Co., Ltd.) at a wavelength of maximum absorbance of Pb(II) (λ_{max}= 479 nm) and MB (λ_{max}= 665 nm).

The removal efficiency and the amount of Pb(II) and MB adsorbed onto M-CHAP/GO were computed using the following equations:

$$q_t = \frac{(C_0 - C_t)V}{m} \quad (1)$$

$$Removal\ efficiency\ (\%) = 100 \times \frac{C_0 - C_e}{C_0} \quad (2)$$

Where C_0 and C_e (mg·L^{-1}) are the initial and equilibrium concentrations of pollutant, respectively. C_t (mg·L^{-1}) is the concentration of adsorbate in aqueous solution at time t (min). q_t (mg·g^{-1}) is the adsorbed amount of adsorbate per unit mass of the adsorbent at time t. V (L) is the volume of adsorbed solution, m (g) is the mass of adsorbent.

2.5 Interference of competing cations

K^+, Na^+, Ca^{2+} and Mg^{2+}, contained in most water, may have competition with Pb(II) on the active sites on the surface of M-CHAP/GO, batch experiments on the interference of competing cations were carried out using KNO_3, $NaNO_3$, $Ca(NO_3)_2$ and $Mg(NO_3)_2$ as the ionic medium in the range of 0-300 mol L^{-1}. All the initial concentration of Pb(II) is 100 mg L^{-1} and the adsorbed volume is 25 mL. Pb(II) was determined by the same spectrophotometry method with adsorption.

3. **Results and discussion**

3.1 Characterization of M-CHAP/GO

3.1.1 SEM and TEM images

Fig. 1 (a) and (b) showed a typical SEM image of the prepared M-CHAP/GO. Fig. 1 (b) was a partial enlargement of Fig. 1 (a) in order to show a better morphology of M-CHAP/GO, especially the GO fold. Fig. 1 (d) displayed the TEM images of M-CHAP/GO for more comprehensive observation of the adsorbent. As expected, spherical M-CHAP successfully loaded onto GO sheet. Magnetic carbonate hydroxyapatite showed a uniform sphere with the average diameter of 65 nm. The sizes distribution and average particle size of M-CHAP can be seen from Fig. 1 (c), which was calculated by the software of Nano Measurer 1.2. GO presented a

sheet-like structure with the large thickness, smooth surface, and wrinkled edge.

After combination, the M-CHAP spheres were uniformly diffused and firmly anchored on the wrinkled GO layers with a high density. Notably, the pleats structure of GO might enable the good distribution of M-CHAP on the surface of GO, meanwhile, the M-CHAP spheres served as a stabilizer separate GO sheets against the aggregation.

3.1.2 Magnetic validation

The magnetic separation effect of the material was demonstrated by a simple laboratory setup with a hand-held magnet as presented in Fig. 1 (e). M-CHAP/GO was well dispersed and remained suspended in aqueous solution during adsorption. When the adsorption reached equilibrium, M-CHAP/GO could be completely separated from the aqueous solution within 1 min at the presence of external magnetic field. Fig. 1 (f) displayed the methylene blue adsorption-separation process. The color of the MB solution treated with M-CHAP/GO was significantly reduced, which indicated the good adsorption properties of M-CHAP/GO.

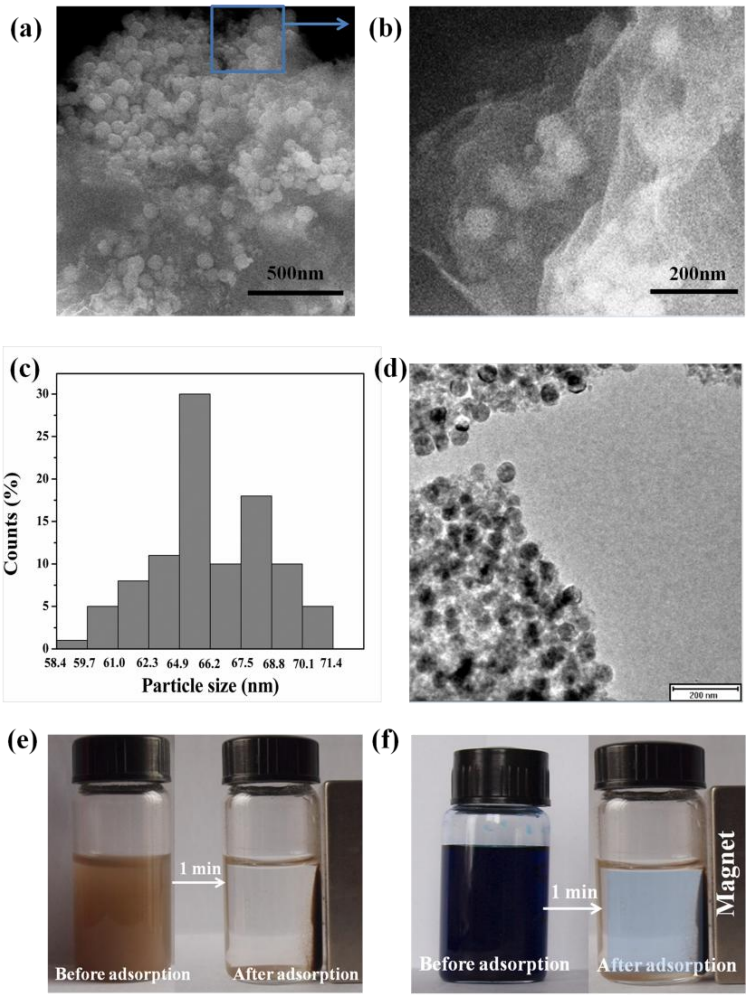

Fig. 1. Characterization of the adsorbent prepared in the study: SEM images (a, b), Particle size distribution (c), TEM images (d) and Demonstration of magnetic separation (e, f)

3.1.3 XRD analysis

Fig. 2 (a) showed the XRD patterns of M-CHAP/GO and its units. The produced reflection patterns match the ICDD standards (JCPDS). The spinel structure of Fe_3O_4, in which the identical peaks for Fe_3O_4 located at 35.5°, 43.1°, 53.4° and 62.6°, correspond to its indices (311), (400), (422) and (400) (NO. 19-0272). GO had a well-defined peak at 10.8° both in the composite of M-CHAP/GO and pure GO[34]. The hexagonal system structure of CHAP identified with its indices (002) and (112), the

other peaks overlapped with Fe_3O_4. Overall, M-CHAP/GO had a good and stable crystal shape.

3.1.4 FTIR spectra

In order to explore the surface characteristics of M-CHAP/GO particles, the FTIR analysis was performed and the spectra were given in Fig. 2 (b). Many peaks of M-CHAP/GO were in conformity with GO sheets and M-CHAP beads. The broadness of the -OH stretching band in the region 3520-3400 cm^{-1} was caused by the adsorbed H_2O and the -OH group on the surface of GO and M-HAP[35]. The bands at 1600-1553 cm^{-1} on M-CHAP/GO and M-CHAP particles were due to CO_3^{2-} incorporation in -OH sites[36]. At the same time, it also contained the characteristic peaks of C=O and C-OH, which often widely appeared in the GO surface[37]. The absorption bands at 582 cm^{-1} were attributed to the Fe-O bond vibration of Fe_3O_4[38]. The peaks at 1008 cm^{-1} and 558 cm^{-1} were well assigned to the molecular vibration of PO_4^{3-}[39]. These oxygen-containing functional groups were conducive to promote the adsorption performance of M-CHAP/GO.

3.1.5 TGA analysis

The thermal behaviors of M-CHAP/GO and its constitute unit were investigated by thermogravmetric analysis (TGA) in dry air (Fig.2 (e)). GO sheets exhibit two steps of mass loss at 200 and 550 $^{\circ}C$ (92%), which are attributed to the removal of oxygen-containing groups and carbon oxidation, respectively. CHAP showed a mass loss at 200 $^{\circ}C$ - 500 $^{\circ}C$ (41%). Fe_3O_4 showed a good thermal stability with just a little loss (9%). The mass loss of M-CHAP/GO (79%) is divided into two stages: the first

part of the curve was most consistent with CHAP at 200 °C - 500 °C and the mass lost was about 36%; the second part was most fit with GO with a mass loss of 48%. After composite, M-CHAP/GO had a better stability performance than the GO alone.

3.1.6 XPS analysis

XPS spectra of survey for the key elements on M-CHAP/GO surfaces were investigated to gain more insights on the construction of prepared adsorbent. From the survey spectra (Fig. 2 (f)), the presence of Fe 2p (710 eV) clearly confirmed the loaded Fe_3O_4 on the surface of M-CHAP/GO. The shark peak of O 1s (527 eV), was attributed to rich oxygen functional groups as well as oxygen atoms in Fe_3O_4. The existence of CHAP was main basis on the peak of Ca 2p (346 eV) and P 2p (133 eV). C 1s (284 eV) was consistent with GO sheet. The elemental analysis results were in conformity with the ideal M-CHAP/GO, and the content of Fe_3O_4, CHAP and GO in M-CHAP/GO was calculated close to 20%, 30% and 50% separately.

3.1.7 BET analysis

According to the N_2 sorption and desorption analysis, the BET surface area of M-CHAP/GO was 105.95 m^2 g^{-1} and BJH desorption cumulative volume of pores was 0.254 cm^3 g^{-1}. The isotherm belonged to the IV type. Adsorption and desorption of curve was steep. Condensation and evaporation occurred at an intermediate relative pressure range. In Fig. 2 (c), isotherm displays a H3 hysteresis loop, indicating the presence of mesopores. Moreover, the observed increase in the hysteresis loops at relative pressures approaching 1.0 suggested the presence of larger mesopores[40]. As a whole, M-CHAP/GO had a slit pore structure of parallel plate.

3.1.8 Zeta potential

Fig. 2 (d) explained the acid-base characteristic of M-CHAP/GO. The pH_{zpc} of M-CHAP/GO, which determines the electrophoretic mobility where the net total particle charge is zero[41], was 3.7 and negatively charged when pH was higher than 3.7. It is reported that the pH of natural water usually ranges from 7 to 9[42]. So, M-CHAP/GO is negatively charged in most of natural water environment.

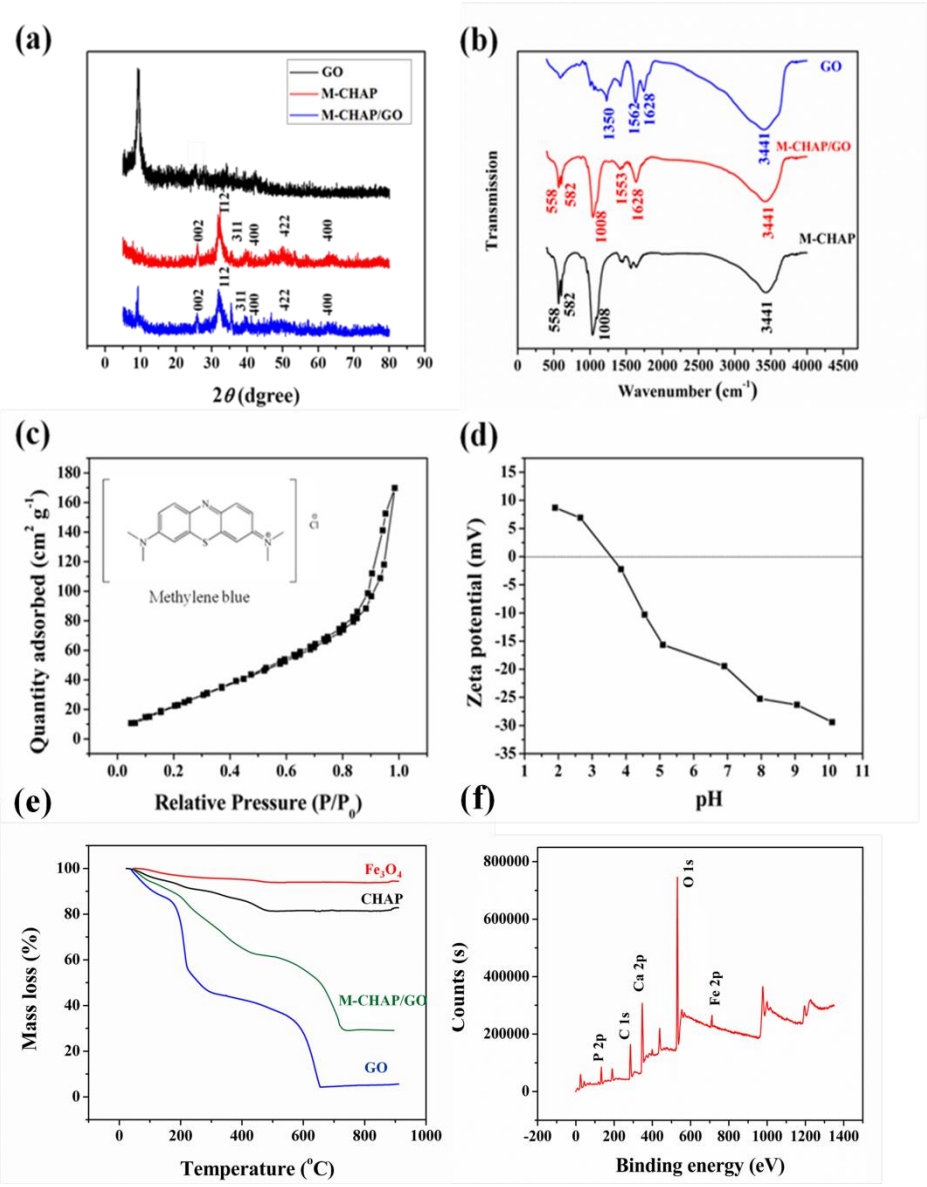

Fig. 2. Characterization of M-CHAP/GO prepared in the study: XRD pattern (a), FTIR pattern (b), BET analysis results (c) and zeta potential (d)

3.2 Factors affecting efficiency of Pb(II) and MB adsorption on M-CHAP/GO

3.2.1 Effect of dosage on the removal efficiency

The 3 h uptake experiments were carried out at 298 K to determine the effect of adsorbent dose. The results in Fig. 3 (a) revealed the removal efficiency increased rapidly with an increasing dosage of adsorbent, which mainly due to the active sites enhanced with an increase amount of M-CHAP/GO. When the dosage was 10 mg, adsorption of Pb(II) approached equilibrium (97.44%) .While the adsorption of MB approached equilibrium (96.43%) at 12 mg. However, an increase in the dosage of M-CHAP/GO does not result in a rise on the removal efficiency for both Pb(II) and MB after the equilibrium, it was because the adsorption reached the saturation state, more amount of adsorbent just made part of adsorption sites turn into waste. Considering the removal efficiency and practicality, 10 mg and 12 mg were selected as the optimum adsorbent dosage for Pb(II) and MB in the following studies.

3.2.2 Effect of pH on the removal efficiency

pH affects the surface charge of an adsorbent as well as the degree of ionization of different pollutants. Thus, the solution pH can greatly affect the adsorption capacity of an adsorbent for heavy metal ions and dye. A series of batch equilibrium tests were carried out to confirm the effect of pH on the removal efficiency at an initial Pb(II) ions concentration of 100 mg L^{-1} and MB concentration of 100 mg L^{-1}. The effect of solution pH was studied in a wide range of 2.0-12.0 as indicated in Fig. 3 (b). Overall, the adsorption capacity of M-CHAP/GO for Pb(II) and MB increased with the increase of pH. Removal efficiency reached the maximum (97.59%) at solution pH

4.5 for Pb(II) ions. This was due to the decrease in competition between positively charged H_3O^+ and Pb(II) for the same adsorption sites on M-CHAP/GO. The adsorption of heavy metals onto M-CHAP/GO mainly relied on the ion-exchange of CHAP. The ion-exchange process can be expressed as follows[19]:

$$Pb^{2+}_{(S)} + \equiv Ca^{2+}_{(H)} \rightarrow \equiv Pb^{2+}_{(H)} + Ca^{2+}_{(S)}$$

Subscripts (S) and (H) denoted solution and M-CHAP/GO phase, respectively. The metals in the solution ($Pb^{2+}_{(S)}$) replaces a surface Ca^{2+} of the adsorbent ($\equiv Ca^{2+}_{(H)}$). The lower pH brought about a large number of H_3O^+, it caused a fierce competition in the ion-exchange sites inside the CHAP. Meanwhile, as pH increased, the protonated hydroxy and carboxyl function groups in GO were deprotonated, enhancing the adsorption capacity of M-CHAP/GO for Pb(II) ions. A further increasing in the solution pH would bring about a decreasing of Pb(II) concentration and other species become primary, such as $PbOH^{+}$[43], which diminished Pb(II) adsorption at solution pH higher than 6.8. Meanwhile, precipitate ($Pb(OH)_2$) could occur at a higher solution pH. Consequently, a pH 4.5 was chosen for further adsorption experiment to avoid the precipitation of $Pb(OH)_2$ above pH 6.8 and the decomposition of adsorbent at an excessive low pH.

The maximum removal efficiency (96.64%) was achieved at solution pH 9.1 for MB. This behavior can be mainly explained by the change in the ionic state of the hydroxy and carboxyl function groups in M-CHAP/GO, which also worked crucially in reaction between M-CHAP/GO and MB. The structure of MB was shown in Fig. 2 (c). MB usually acted as a positive ion (MB^+) in the aqueous solution. So, the

negative surface charge of the adsorbent would be beneficial to the removal of MB. When the solution pH was low, functional groups were protonated. The electrostatic attraction between M-CHAP/GO and MB weakened. As a result, MB uptake capacity decreased. When the solution pH increased gradually, hydroxy and carboxyl function groups were deprotonated and MB^+ can be bound to negatively charged groups by electrostatic attraction. To make sure the maximum removal efficiency, all the following experiments were carried out at solution pH 9.1 for MB.

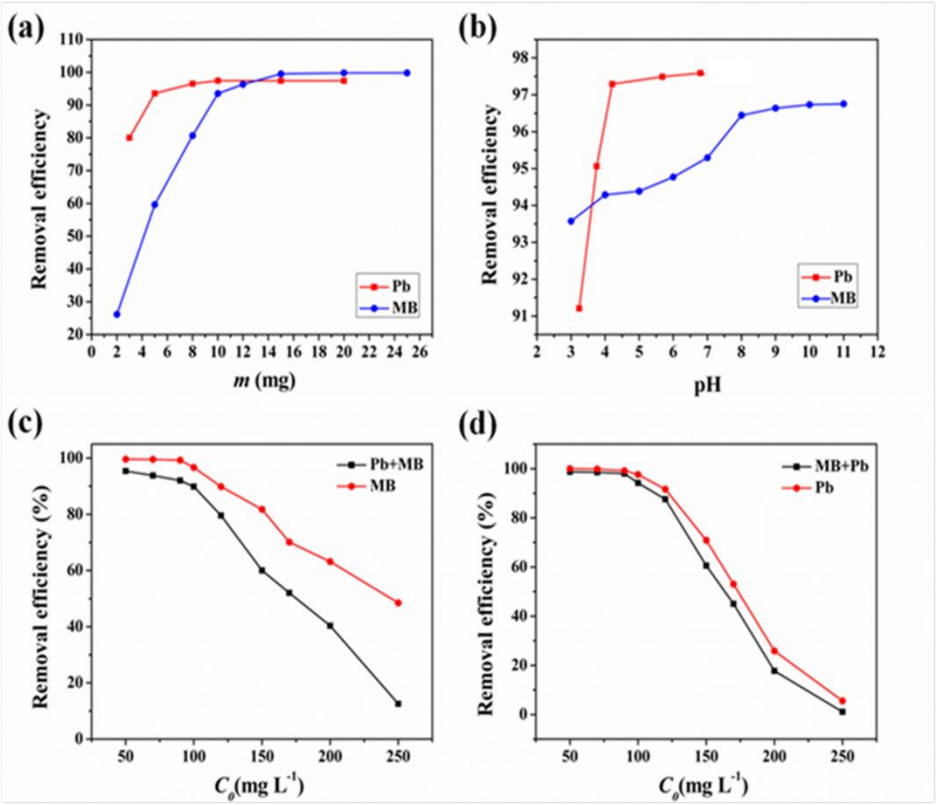

Fig. 3. Effect of dosage (a), pH (b) and initial concentration (c, d) on adsorption behavior of MB and Pb(II) (V=25 mL, t=3 h, temperature at 298 K)

3.2.3 Effect of initial concentration on the removal efficiency

When the aqueous solution containing heavy metals and dye, it would be very meaningful for the adsorbent to adsorb them at the same time and maintain good

removal efficiency. Fig. 3 (c) and (d) showed the adsorption capacity of M-CHAP/GO for Pb(II) and MB in the different initial concentration as well as the mutual influence between them. Fig. 3 (c) showed the effect of initial Pb(II) concentration on the removal efficiency of MB. The presence of Pb(II) ions caused a weak influence on the adsorption of MB onto M-CHAP/GO. It was because the adsorption of MB mainly dependent on the abundant functional groups on the surface of GO, but Pb(II) ions could also come into electrostatic effect with these functional groups, so as to produce certain competition with MB on the adsorption sites. Fig. 3 (d) implied the effect of initial MB concentration on the removal efficiency of Pb(II) ions. MB in the aqueous solution didn't affect the adsorption efficiency of Pb(II) ions. The ion-exchange effect of CHAP was the crucial mechanism of Pb(II) ions adsorption. The role of functional groups was not too essential, and Pb(II) didn't have intense competition with MB. So, the removal efficiency of Pb(II) was generally not influenced by MB.

3.2.4 Effect of contact time on the removal efficiency and adsorption kinetics

For the design and optimization of a wastewater treatment plant, the effect of contact time on the adsorption capacity of M-CHAP/GO for pollutants was carried out at solution pH 4.5 for Pb(II) and pH 9.1 for MB. The results were shown in Fig. 4 (a). The increase in removal efficiency with increasing contact time was attributed to more available time for pollutants to interaction with adsorption sites on the surface or inside M-CHAP/GO. It took 30 min for Pb(II) and 90 min for MB to reach equilibrium. The phenomenon might be explained by the smaller size of heavy metals than that of organic molecules. In the following experiments, 30 and 90 min were

selected as the suitable contact time for Pb(II) and MB.

To further analyze the adsorption kinetics, the pseudo-first-order equation, pseudo-second-order equation, Elovich equation, intraparticle diffusion equation and Bangham equation were applied to describe the kinetics of Pb(II) and MB adsorbing onto M-CHAP/GO. Each model is expressed as follows:

(1) Pseudo-first-order model:

$$\lg(q_e - q_t) = \lg q_e - k_1 t \quad (3)$$

(2) Pseudo-second-order model:

$$\frac{t}{q_t} = \frac{1}{k_2 q_e^2} + \frac{t}{q_e} \quad (4)$$

(3) Elovich model:

$$q_t = \frac{1}{\beta}\ln(\alpha \cdot \beta) + \frac{1}{\beta}\ln t \quad (5)$$

(4) Intraparticle diffusion model:

$$q_t = k_{dif} t^{1/2} + C \quad (6)$$

(5) Bangham model:

$$\ln q_t = \ln k_b + (\frac{1}{m})\ln t \quad (7)$$

where q_e and q_t (mg g^{-1}) are the adsorbed amount of pollutants onto adsorbent at equilibrium and at time t (min), respectively. k_1 and k_2 (mg min g^{-1}) are the pseudo-first-order and pseudo-second-order rate constant. α (mmol g^{-1} min^{-1}) is the initial adsorption rate and β (g $mmol^{-1}$) is the desorption constant. k_{dif} (mg g^{-1} $min^{-1/2}$) is the intraparticle diffusion rate constant. m and k_b are the related constant of Bangham model.

The linear fitting results of kinetics were shown in Fig. 4 and the relevant calculative results were listed in Table. 1. The pseudo-second-order kinetic model gave a satisfactory fit to all the experimental data compared to other kinetic models for Pb(II) (R^2=0.9999) and MB (R^2=0.9998), which mean that the main rate determining step was chemisorptions. That is to say, the overall rate of Pb(II) and MB adsorption process seemed to be controlled by the chemical process through exchanging of electrons or a chemical reaction between adsorbent and adsorbates[44]. Besides, the calculated q_e according to pseudo-second-order kinetic model was 244.5 mg g^{-1} for Pb(II) and 409.8 mg g^{-1} for MB, which were consistent with the experimental data (244.2 mg g^{-1} for Pb(II) and 403.7 mg g^{-1} for MB).

In addition, the linear fitting results of the MB adsorption process was in conformity with the intraparticle diffusion model, which indicated the MB adsorption process could be explained by the following three portions[45]: (Ⅰ) the first portion corresponded to boundary layer diffusion or external surface adsorption, about 25 min; (Ⅱ) the second stage was a gradual adsorption stage attributed to intraparticle diffusion, about 65 min; (Ⅲ) the final plateau region was equilibrium adsorption. For MB removal by M-CHAP/GO, the intraparticle process might be another rate-limiting step.

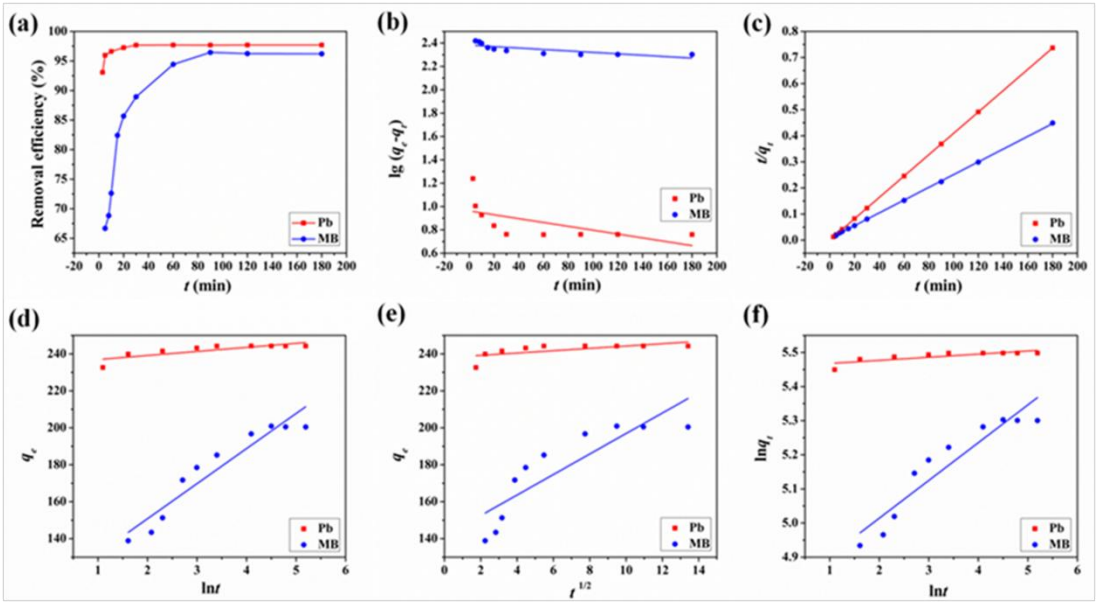

Fig. 4. Effect of contact time on the removal efficiency (a), Pseudo-first-order kinetics (b), Pseudo-second-order kinetics (c), Elovich kinetics (d), Intraparticle diffusion kinetics (e) and Bangham kinetics (f) for adsorption of Pb(II) and MB onto M-CHAP/GO. (C_0=100 mg L^{-1}, V=25 mL, t=3–180 min, temperature at 298 K)

Table 1. Constants and correlation coefficients for the kinetic models

Kinetic model	Parameder	Pb(II)	R^2	MB	R^2
Pseudo-first-order	k_1 (mg min g^{-1})	0.001655	0.3757	0.0006174	0.5642
	q_e (mg g^{-1})	29.87		241.3	
Pseudo-second-order	k_2 (mg min g^{-1})	0.04508	0.9999	0.008556	0.9998
	q_e (mg g^{-1})	244.5		409.8	
Elovich	α (mmol g^{-1} min^{-1})	8.066	0.6291	7.268	0.8256
	β (g $mmol^{-1}$)	0.4567		0.05269	
Intraparticle diffusion	k_{dif} (mg g^{-1} $min^{-1/2}$)	0.6309	0.3774	5.5445	0.9253
Bangham	m	0.5839	0.6236	0.6086	0.8736
	k_b (mg g^{-1})	1.025		1.275	

3.3 Adsorption isotherms

When the adsorption occurs, the progress will proceed until the remaining adsorbate is in dynamic equilibrium with that on the adsorbent surface. Adsorption isotherms can provide some physicochemical information on how the adsorption proceeds and how adsorbate interacts with adsorbent surface[46]. The adsorption behavior was described by four common adsorption models as follow:

(1) Henry equation:

$$q_e = K_H C_e \tag{8}$$

(2) Langmuir equation:

$$\frac{1}{q_e} = \frac{1}{bq_m}\frac{1}{C_e} + \frac{1}{q_m} \tag{9}$$

(3) Freundlich equation:

$$\ln q_e = \ln K_F + \frac{1}{n}\ln C_e \tag{10}$$

(4) Temkin equation:

$$q_e = \frac{RT}{b_T}\ln C_e + \frac{RT}{b_T}\ln A_T \tag{11}$$

where q_m is the maximum adsorption capacity (mg g^{-1}). K_H and K_F are the constants that are related to the adsorption capacity and intensity. b is the adsorption intensity or Langmuir coefficient related to the affinity of the binding site (L mg^{-1}). A smaller $1/n$ value indicates a more heterogeneous surface whereas a value closer to or equal to one indicates the adsorbent has relatively more homogeneous binding sites. $\frac{RT}{b_T}$ is related to the adsorption heat. A_T is the equilibrium constant corresponding to the maximum binding-energy.

The four common adsorption models showed in Fig. 5 .The isotherm parameters

calculated from the slope and intercept of Fig. 5 and presented in Table 2. Taking the correlation coefficient as a criterion for good fit of the system, the equilibrium adsorption data were well fitted Langmuir model for both Pb(II) (R^2 = 0.9645, R^2 = 0.9547, R^2 = 0.8984) and MB (R^2 = 0.9943, R^2 = 0.9549, R^2 = 0.9538) at 298 K, 308 K and 318 K. The Langmuir isotherm indicated that the surface of M-CHAP/GO was monolayer covered with Pb(II) or MB[47]. According to the Langmuir isotherm parameters, the maximum adsorption capacity of M-CHAP/GO nano-particles for Pb(II) and MB was 277.7 mg g^{-1} and 546.4mg g^{-1} at 318 K, respectively. $0 < 1/n < 0.5$ indicated that Pb(II) or MB was facile to be adsorbed onto M-CHAP/GO. Furthermore, the correlation coefficients for Temkin isotherm model of Pb(II) and MB adsorption onto M-CHAP/GO were all higher than 0.9285 at the three temperature, which revealed that the adsorption system based on the heat[48]. Table. 2 also presented that the adsorption capacity from experiment significantly increased with the increase of temperature. It could be explained from two aspects: Firstly, an increase in temperature is known to increase the diffusion rate of the adsorbate across the external boundary layer and within the pores of the porous adsorbent[49]. So, the adsorption capacity increased, especially for heavy metals; Secondly, more bond ruptures of the functional groups on the adsorbent surface at a higher temperature may increase the number of active adsorption sites, it also contributes to an enhanced adsorption capacity of the adsorbent.

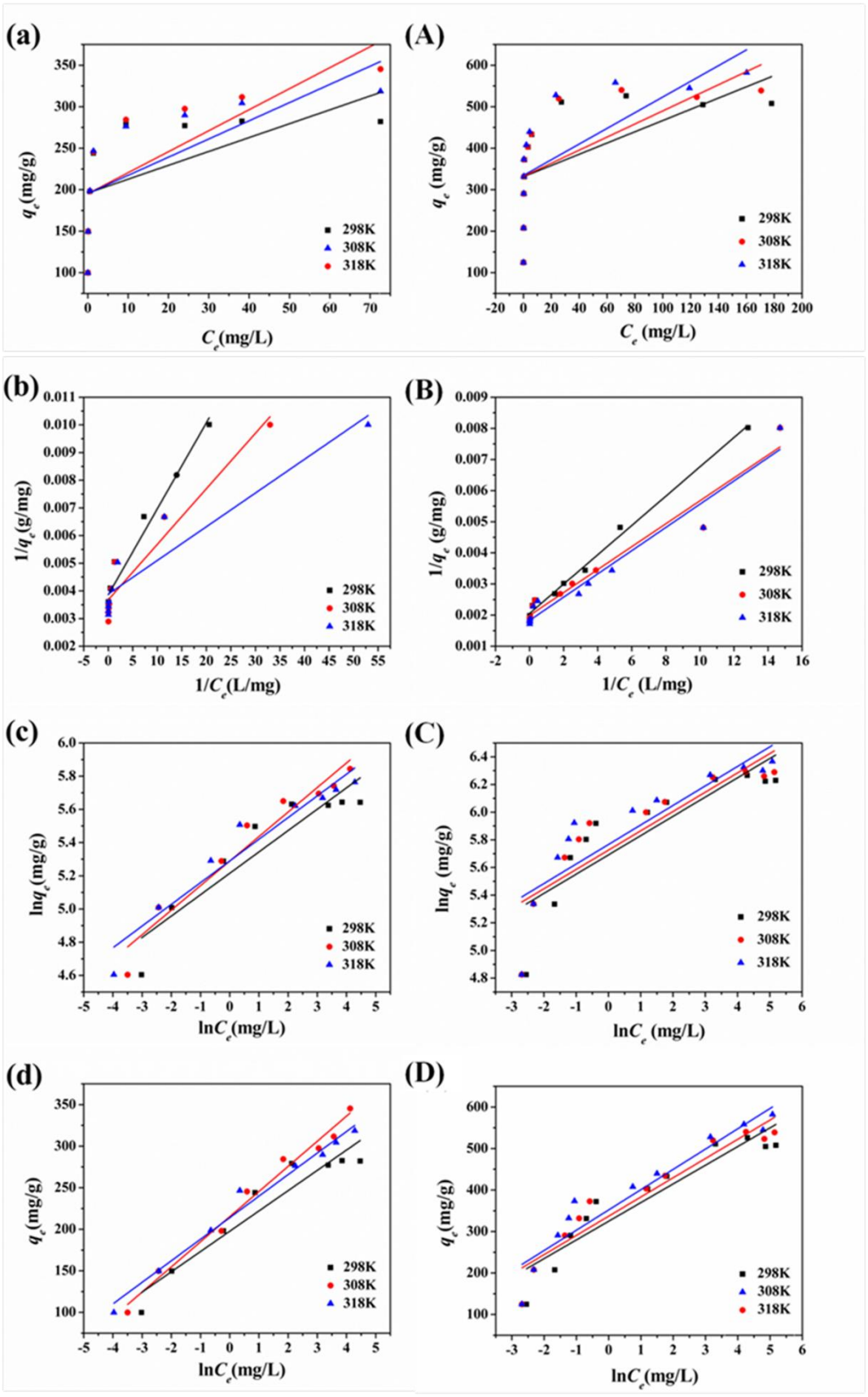

Fig. 5. Henry (a), Langmuir (b), Freundlich (c), and Temkin (d) adsorption

isotherm fit of Pb(II) onto M-CHAP/GO (C_0=40−200 mg L^{-1}, V=25 mL, contact time for 30 min, pH at 4.5, temperature at 298 K, 308 K and 318 K) and Henry (A), Langmuir (B), Freundlich (C), and Temkin (D) adsorption isotherm fit of MB onto M-CHAP/GO (C_0=30−300 mg L^{-1}, V=25 mL, contact time for 90 min, pH at 9.1, temperature at 298 K, 308 K and 318 K)

Table 2. Adsorption isotherm parameters for Pb(II) and MB adsorption onto M-CHAP/GO at 298 K, 308 K, 318 K

Temperature	Adsorption isotherm	Parameter	Pb(II)	R^2	MB	R^2
298 K	Henry	K_H	1.871	0.5773	1.355	0.5281
	Langmuir	b	12.41	0.9645	4.375	0.9943
		q_m	246.1		405.4	
	Freundlich	K_F	184.1	0.8422	296.4	0.7161
		$1/n$	0.1287		0.1393	
	Temkin	b_T	215.3	0.9812	352.2	0.9399
		A_T	1235		1348	
308 K	Henry	K_H	2.530	0.6239	1.577	0.5846
	Langmuir	b	18.34	0.9547	5.516	0.9549
		q_m	271.7		502.5	
	Freundlich	K_F	198.1	0.9151	307.7	0.7443
		$1/n$	0.1478		0.1396	
	Temkin	b_T	213.9	0.9285	324.9	0.9645
		A_T	3849		1370	
318 K	Henry	K_H	2.191	0.5431	1.891	0.6469
	Langmuir	b	31.84	0.8984	5.901	0.9538
		q_m	277.7		546.4	
	Freundlich	K_F	198.4	0.8811	319.5	0.7312
		$1/n$	0.1307		0.1412	
	Temkin	b_T	197.7	0.9551	337.2	0.9493
		A_T	3287		1448	

3.4 Adsorption thermodynamic

To further evaluate the effect of temperature influence on the adsorption and investigate the possible mechanism involved in the adsorption progress, the thermodynamic behaviors were evaluated by the following equations:

$$\Delta G = -RT \ln K_d \quad (12)$$

$$\ln K_d = \frac{\Delta S}{R} - \frac{\Delta H}{RT} \quad (13)$$

where R (8.314 J mol^{-1} K^{-1}) is the gas constant, T (K) is the absolute temperature and K_d is the thermodynamic equilibrium constant. ΔS is the entropy change, ΔH is the enthalpy change and ΔG is the Gibbs free energy change in a given process (kJ mol^{-1}), respectively. The results of ΔS, ΔH and ΔG were shown in Table. 3. All the values of ΔG at three temperatures were negative, which indicated the feasibility of the process and spontaneous nature of the adsorption. These increased values with the increasing temperature mean a better adsorption performance at a higher temperature. Furthermore, the positive values of ΔH calculated from the fitting line in Fig. 6 are high enough to ensure the strong interaction between adsorbent and adsorbates. And also, the positive value of ΔS implied an increased randomness at the solid-solution interface with the increase of temperature.

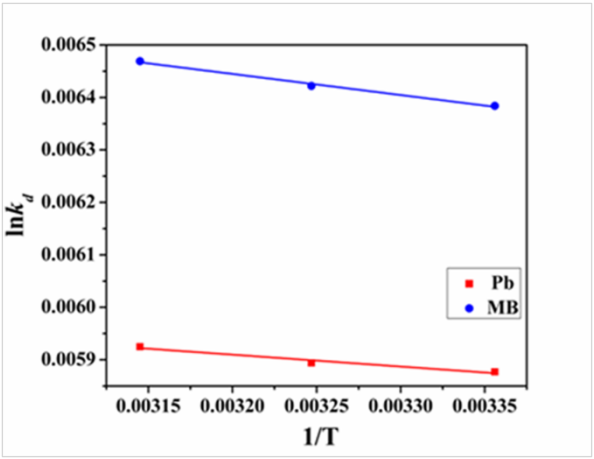

Fig. 6. Thermodynamics fittings for Pb(II) onto M-CHAP/GO (C_0=100 mg L^{-1},

V=25 mL, contact time for 30 min, pH at 4.5) and MB onto M-CHAP/GO (C_0=100 mg L^{-1}, *V*=25 mL, contact time for 90 min, pH at 9.1)

Table 3. Thermodynamic parameters for Pb(II) and MB adsorption onto M-CHAP/GO

Pollutants	Temperature	lnK_d	ΔG (kJ mol^{-1})	ΔH (kJ mol^{-1})	ΔS (J mol^{-1} K^{-1})
Pb(II)	298 K	0.005877	-14.56	1.885	55.21
	308 K	0.005894	-15.09		
	318 K	0.005925	-15.66		
MB	298 K	0.006384	-15.81	3.372	64.27
	308 K	0.006422	-6.44		
	318 K	0.006469	-17.11		

3.5 Effect of ionic strength on adsorption

Generally, wastewaters from industries contain cations such as K^+, Na^+, Ca^{2+} and Mg^{2+}, they have similar physical and chemical properties with heavy metal ions, thus, their presence in aqueous solution may compete with Pb(II) on the adsorption sites in M-CHAP/GO and thus affect the adsorption capacity. In order to investigate the effect of K^+, Na^+, Ca^{2+} and Mg^{2+} on Pb(II) adsorption, the competing experiments were carried out using KNO_3, $NaNO_3$, $Ca(NO_3)_2$ and $Mg(NO_3)_2$ as cations source in a range of 0-300 mol L^{-1}. From the tested data shown in Fig. 7, the removal efficiency of Pb(II) reduced less than 1% with the presence of K^+, Na^+, Ca^{2+} and Mg^{2+} in the solution. Compared with K^+ and Na^+, Ca^{2+} and Mg^{2+} resulted in a little larger reduction on the adsorption capacity of Pb(II). It is because Ca^{2+}, Mg^{2+} and Pb^{2+} are bivalent cations, they have more similar physical and chemical properties. On the whole, K^+, Na^+, Ca^{2+} and Mg^{2+} had a little effect on the adsorption of Pb(II) onto M-CHAP/GO.

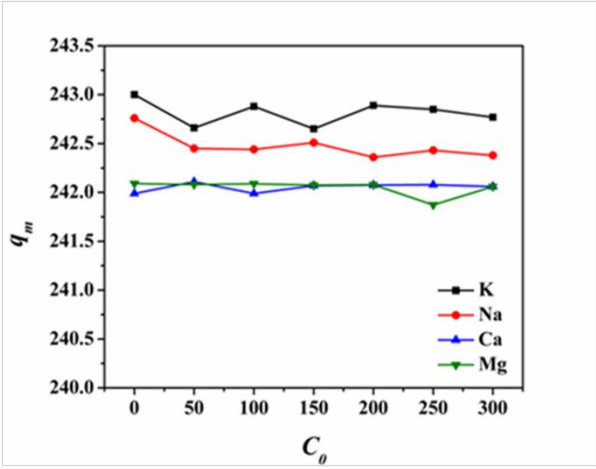

Fig. 7. Effect of ionic strength on adsorption (*m*=10 mg, *V*=25 mL, *t*=3 h, pH at 4.5, temperature at 298 K)

3.6 Adsorption capacity comparison of different composition unit

Sole M-GO and M-CHAP samples were prepared to compare the adsorption capacity difference in Pb(II) and MB. In Fig. 8, adsorption results compared M-CHAP with M-CHAP/GO can be found that M-CHAP play a major role in the adsorption of Pb(II). Similar to this, comparison of M- GO and M-CHAP/GO implied that M-GO mainly worked in the adsorption of MB. A combination of M-CHAP and M-GO make M-CHAP/GO has a good adsorption performance in the removal of both heavy metals and dyes.

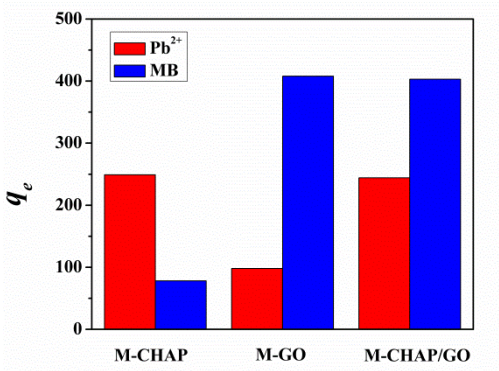

Fig. 8. Comparison of the different capacity in Pb(II) and MB adsorption

3.7 Performance evaluations

Various adsorbents have been reported for removal of heavy metal ions or dye. Table. 4 listed the comparison of the maximum adsorption capacities (q_m) of M-CHAP/GO with other adsorbents in literature for heavy metal ions or dye adsorption. Considering whether q_m or the simple feasibility, M-CHAP/GO showed superior performance. Some composite adsorbents perform better for one or two contaminants, but they have an expensive or complex synthetic process. Taking the economic cost and applied scope into consideration, M-CHAP/GO has a better prospect in adsorption or other field.

Table 4. Adsorption capacities of various adsorbents

Material	Target element	Isotherm	Kinetic	q_m (mg g^{-1})	Ref.
MCD-GO-R	Pb(II) Methylene blue	Langmuir	PSO	277.7 546.4	This paper
Chitosan spheres	Hg(II)	Langmuir	PSO	31.1	[50]
Fe_3O_4-cyclodextrin	Pb(II) Cd(II) Ni(II)	Langmuir	PSO	64.5 27.7 13.2	[51]
Ion exchange resins	Hg(II)	Freundlich	PSO	215.75	[52]
Chitosan beads-supported Fe^0-nanoparticles	Cu(II) Pb(II) Cr(VII) Cd(II)	- - - -	- - - -	55.19 22.66 55.96 30.75	[53]
Fe_3O_4@SiO_2-NH_2	Pb(II)	Langmuir	PSO	243.9	[54]
Polyethersulfone /hydrous manganese dioxide	Pb(II)	Langmuir Freundlich	PSO	204.1	[55]
Activated carbon	Methylene blue	Langmuir	PSO	454.2	[56]
Commercial activated carbon	Methylene blue	Langmuir Freundlich	B-V I-D Lagergren	298.9	[57]
Tea waste	Methylene blue	Langmuir	PSO	85.16	[58]
Oil palm fibre activated carbon	Methylene blue	Langmuir	PSO	277.8	[59]

Cinnamomum camphora sawdust	Malachite green	Langmuir Freundlich Temkin	PSO	157.5	[60]
Aamino functionalized graphenes	Metanil yellow	Langmuir	PSO	71.6	[61]

4. Conclusions

In this work, M-CHAP/GO was prepared through two steps: M-CHAP was first synthesized by the coprecipitation method and then loaded onto graphene oxide sheet. M-CHAP/GO performed well on the adsorption of Pb(II) and MB. The equilibrium adsorption capacity was 277.7 mg g^{-1} for Pb(II) and 546.4 mg g^{-1} for MB at 308 K. The pseudo-second-order equation and the Langmuir model were found to fit the experimental data for both contaminants. The adsorption process was efficient and rapid. Furthermore, the thermodynamic studies illustrated that the adsorption process was endothermic and spontaneous in nature, which showed a good economic efficiency. In terms of high efficiency and feasibility, M-CHAP/GO could be a promising absorbent for removing heavy metals and dye from aqueous solution.

Acknowledgments

This study was supported by the National Natural Science Foundation of China (No. 21175057, 21375047 and 21377046), the Science and Technology Plan Project of Jinan (No. 201307010), and QW thanks the Special Foundation for Taishan Scholar Professorship of Shandong Province and UJN (No. ts20130937).

References:

1. X. Yang, C. Chen, J. Li, G. Zhao, X. Ren and X. Wang, *RSC Advances*, 2012, 2, 8821-8826.
2. G. Zhao, J. Li, X. Ren, C. Chen and X. Wang, *Environmental Science & Technology*, 2011, 45, 10454-10462.
3. L. Järup, *British Medical Bulletin*, 2003, 68, 167-182.
4. V. K. Gupta, M. Gupta and S. Sharma, *Water Research*, 2001, 35, 1125-1134.
5. I. Tan, A. L. Ahmad and B. Hameed, *Journal of Hazardous Materials*, 2008, 154, 337-346.
6. D. Ghosh and K. G. Bhattacharyya, *Applied Clay Science*, 2002, 20, 295-300.
7. D. Manohar, K. Anoop Krishnan and T. Anirudhan, *Water Research*, 2002, 36, 1609-1619.
8. Y. Sun, C. Chen, D. Shao, J. Li, X. Tan, G. Zhao, S. Yang and X. Wang, *RSC Advances*, 2012, 2, 10359-10364.
9. M. Srinivasan, C. Ferraris and T. White, *Environmental Science & Technology*, 2006, 40, 7054-7059.
10. Y. Xu, F. W. Schwartz and S. J. Traina, *Environmental Science & Technology*, 1994, 28, 1472-1480.
11. R. Sheha, *Journal of Colloid and Interface Science*, 2007, 310, 18-26.
12. Y. Li, C. Liu, H. Zhai, G. Zhu, H. Pan, X. Xu and R. Tang, *RSC Advances*, 2014, 4, 25398-25403.
13. X. Chen, J. V. Wright, J. L. Conca and L. M. Peurrung, *Environmental Science*

& Technology, 1997, 31, 624-631.

14. P. K. Chaturvedi, C. S. Seth and V. Misra, *Chemosphere*, 2006, 64, 1109-1114.
15. S. McGrellis, J.-N. Serafini, J. JeanJean, J.-L. Pastol and M. Fedoroff, *Separation and Purification Technology*, 2001, 24, 129-138.
16. J. C. Seaman, J. S. Arey and P. M. Bertsch, *Journal of Environmental Quality*, 2001, 30, 460-469.
17. K. Elkabouss, M. Kacimi, M. Ziyad, S. Ammar and F. Bozon-Verduraz, *Journal of Catalysis*, 2004, 226, 16-24.
18. A. G. Leyva, J. Marrero, P. Smichowski and D. Cicerone, *Environmental Science & Technology*, 2001, 35, 3669-3675.
19. D. Liao, W. Zheng, X. Li, Q. Yang, X. Yue, L. Guo and G. Zeng, *Journal of Hazardous Materials*, 2010, 177, 126-130.
20. W. Zheng, X. Li, Q. Yang, G. Zeng, X. Shen, Y. Zhang and J. Liu, *Journal of Hazardous Materials*, 2007, 147, 534-539.
21. B. Ma, W. S. Shin, S. Oh, Y.-J. Park and S.-J. Choi, *Separation Science and Technology*, 2010, 45, 453-462.
22. Z. Xu and J. Dong, *Emerging Environmental Technologies*, 2008, 278, 105-148.
23. J. Gómez-Pastora, E. Bringas and I. Ortiz, *Chemical Engineering Journal*, 2014, 256, 187-204.
24. S. Zhang, J. Li, T. Wen, J. Xu and X. Wang, *RSC Advances*, 2013, 3, 2754-2764.

25. X. Guo, B. Du, Q. Wei, J. Yang, L. Hu, L. Yan and W. Xu, *Journal of Hazardous Materials*, 2014, 278, 211-220.

26. S. Wang, Y. Boyjoo and A. Choueib, *Chemosphere*, 2005, 60, 1401-1407.

27. T. Robinson, B. Chandran and P. Nigam, *Water Research*, 2002, 36, 2824-2830.

28. G. Sheng, Y. Li, X. Yang, X. Ren, S. Yang, J. Hu and X. Wang, *RSC Advances*, 2012, 2, 12400-12407.

29. G. Ramesha, A. Vijaya Kumara, H. Muralidhara and S. Sampath, *Journal of Colloid and Interface Science*, 2011, 361, 270-277.

30. C. J. Madadrang, H. Y. Kim, G. Gao, N. Wang, J. Zhu, H. Feng, M. Gorring, M. L. Kasner and S. Hou, *ACS Applied Materials & Interfaces*, 2012, 4, 1186-1193.

31. L. Ai, C. Zhang and Z. Chen, *Journal of Hazardous Materials*, 2011, 192, 1515-1524.

32. L. Sun, H. Yu and B. Fugetsu, *Journal of Hazardous Materials*, 2012, 203, 101-110.

33. S. Guo, D. Li, L. Zhang, J. Li and E. Wang, *Biomaterials*, 2009, 30, 1881-1889.

34. H. Su, Z. Li, Q. Huo, J. Guan and Q. Kan , *RSC Advances*, 2014, 4, 9990-9996.

35. C. C. Ribeiro, I. Gibson and M. A. Barbosa, *Biomaterials*, 2006, 27, 1749-1761.

36. Z. H. Cheng, A. Yasukawa, K. Kandori and T. Ishikawa, *Journal of the Chemical Society, Faraday Transactions*, 1998, 94, 1501-1505.

37. P. Kumar, G. Singh, D. Tripathi and S. L. Jain , *RSC Advances*, 2014, 4, 50331-50337.

38. S. Li, H. Bai, J. Wang, X. Jing, Q. Liu, M. Zhang, R. Chen, L. Liu and C. Jiao, *Chemical Engineering Journal*, 2012, 193, 372-380.

39. K. Lin, P. Liu, L. Wei, Z. Zou, W. Zhang, Y. Qian, Y. Shen and J. Chang, *Chemical Engineering Journal*, 2013, 222, 49-59.

40. J. Zhou, C. Tang, B. Cheng, J. Yu and M. Jaroniec, *ACS Applied Materials & Interfaces*, 2012, 4, 2174-2179.

41. G. Moussavi and B. Barikbin, *Chemical Engineering Journal*, 2010, 162, 893-900.

42. C. Belin, C. Quellec, M. Lamotte, M. Ewald and P. Simon, *Environmental Technology*, 1993, 14, 1131-1144.

43. V. K. Gupta, M. Gupta and S. Sharma, *Water Research*, 2001, 35, 1125-1134.

44. A. Mohammadi, H. Daemi and M. Barikani, *International Journal of Biological Macromolecules*, 2014.

45. J. H. Chen, Q. L. Liu, S. R. Hu, J. C. Ni and Y. S. He, *Chemical Engineering Journal*, 2011, 173, 511-519.

46. C. Ng, J. N. Losso, W. E. Marshall and R. M. Rao, *Bioresource Technology*, 2002, 85, 131-135.

47. L. Wang, J. Zhang and A. Wang, *Desalination*, 2011, 266, 33-39.

48. E. Malkoc, *Journal of Hazardous Materials*, 2006, 137, 899-908.

49. J. H. Chen, H. T. Xing, H. X. Guo, G. P. Li, W. Weng and S. R. Hu, *Journal of Hazardous Materials*, 2013, 248, 285-294.

50. R.S. Vieira, M.M. Beppu, *Water Research*, 2006, 40, 1726-1734.

51. A.Z.M. Badruddoza, Z.B.Z. Shawon, W.J.D. Tay, K. Hidajat, M.S. Uddin, *Carbohydrate polymers*, 2013, 91, 322-332.

52. S. Chiarle, M. Ratto, M. Rovatti, *Water Research*, 2000, 34, 2971-2978.

53. T. Liu, X. Yang, Z.L. Wang, X.X. Yan, *Water Research*, 2013, 47, 6691-6700.

54. J. Zhang, S. Zhai, S. Li, Z. Xiao, Y. Song, Q. An, G. Tian, *Chemical Engineering Journal*, 2013, 215 461-471.

55. R. Jamshidi Gohari, W. Lau, T. Matsuura, E. Halakoo, A. Ismail, *Separation and Purification Technology*, 2013, 120, 59-68.

56. B. Hameed, A.M. Din, A. Ahmad, *Journal of Hazardous Materials*, 2007, 141, 819-825.

57. N. Kannan, M.M. Sundaram, *Dyes and Pigments*, 2001, 51, 25-40.

58. M.T. Uddin, M.A. Islam, S. Mahmud, M. Rukanuzzaman, *Journal of Hazardous Materials*, 2009, 162, 53-60.

59. I. Tan, B. Hameed, A. Ahmad, *Chemical Engineering Journal*, 2007, 127, 111-119.

60. H. Wang, X. Yuan, G. Zeng, L. Leng, X. Peng, K. Liao, L. Peng, Z. Xiao, *Environmental Science and Pollution Research*, 2014, 1-13.

61. X. Guo, Q. Wei, B. Du, Y. Zhang, X. Xin, L. Yan, H. Yu, *Applied Surface*

Science, 2013, 284, 862-869.